



HAL
open science

Crystal Structures of Ternary Ruthenium Ferrites $\text{SrM}_{2\pm x}\text{Ru}_{4\pm x}\text{O}_{11}$ with $M = \text{Fe}, \text{Co}$ and Magnetic and Transport Properties of Al-doped Single Crystals

Rainer Niewa, Larysa Shlyk, Barbara Schüpp-Niewa, Lance E. de Long

► **To cite this version:**

Rainer Niewa, Larysa Shlyk, Barbara Schüpp-Niewa, Lance E. de Long. Crystal Structures of Ternary Ruthenium Ferrites $\text{SrM}_{2\pm x}\text{Ru}_{4\pm x}\text{O}_{11}$ with $M = \text{Fe}, \text{Co}$ and Magnetic and Transport Properties of Al-doped Single Crystals. *Journal of Inorganic and General Chemistry / Zeitschrift für anorganische und allgemeine Chemie*, 2009, 636 (2), pp.331. 10.1002/zaac.200900308 . hal-00512582

HAL Id: hal-00512582

<https://hal.science/hal-00512582>

Submitted on 31 Aug 2010

HAL is a multi-disciplinary open access archive for the deposit and dissemination of scientific research documents, whether they are published or not. The documents may come from teaching and research institutions in France or abroad, or from public or private research centers.

L'archive ouverte pluridisciplinaire **HAL**, est destinée au dépôt et à la diffusion de documents scientifiques de niveau recherche, publiés ou non, émanant des établissements d'enseignement et de recherche français ou étrangers, des laboratoires publics ou privés.



**Crystal Structures of Ternary Ruthenium Ferrites
 $\text{SrM}_{2\pm x}\text{Ru}_{4\pm x}\text{O}_{11}$ with $M = \text{Fe, Co}$ and Magnetic and Transport
 Properties of Al-doped Single Crystals**

Journal:	<i>Zeitschrift für Anorganische und Allgemeine Chemie</i>
Manuscript ID:	zaac.200900308.R1
Wiley - Manuscript type:	Article
Date Submitted by the Author:	03-Jul-2009
Complete List of Authors:	Niewa, Rainer; Universität Stuttgart, Anorganische Chemie Shlyk, Larysa; University of Kentucky, Department of Physics and Astronomy Schüpp-Niewa, Barbara; Universität Stuttgart, Anorganische Chemie De Long, Lance E.; University of Kentucky, Department of Physics and Astronomy
Keywords:	Ruthenates, Oxides, Ferromagnetic Semiconductors



ARTICLE

DOI: 10.1002/zaac.200((will be filled in by the editorial staff))

Crystal Structures of Ternary Ruthenium Ferrites $\text{SrM}_{2\pm x}\text{Ru}_{4\mp x}\text{O}_{11}$ with $M = \text{Fe}, \text{Co}$ and Magnetic and Transport Properties of Al-doped Single Crystals

Rainer Niewa,^{*[a,b]} Larysa Shlyk,^[c] Barbara Schüpp-Niewa,^[a] Lance E. De Long,^[c]

Dedicated to Prof. Dr. Hans-Jörg Deiseroth on the Occasion of his 65th birthday

Keywords: Ruthenates, Oxides, Ferromagnetic Semiconductors

Single crystals of $\text{SrM}_{2\pm x}\text{Ru}_{4\mp x}\text{O}_{11}$ with $M = \text{Fe}, \text{Co}$ with maximum width 2 mm and thickness around 0.05 mm were grown from a chloride flux. Sample compositions were determined from refinements of X-ray diffraction data and microprobe analysis. The hexagonal crystal structure (space group $P6_3/mmc$, $Z = 2$) consists of basal-plane layers of edge-sharing octahedra $(M,\text{Ru})\text{O}_6$, which are connected along [001] by face-sharing pairs of octahedra $(M,\text{Ru})_2\text{O}_9$ and trigonal bipyramids MO_5 . A significant homogeneity range is generated by variable occupation of the octahedral sites by 3d and 4d elements. Al is also found to substitute for transition elements in the octahedral sites. The title compounds are narrow-gap semiconductors and soft ferromagnets with Curie temperatures that can substantially exceed room-temperature, depending on composition. Al doping significantly modifies the transport properties, but magnetic properties such as the Curie temperature, magnetization and anisotropy are less affected. Hall coefficient measurements reveal the predominant charge carriers are holes. The structural, electronic and magnetic properties suggest that these solid solutions are promising candidates for spin-injection devices.

* Institut für Anorganische Chemie, Universität Stuttgart, Pfaffenwaldring 55, 70569 Stuttgart, Germany
Fax: +49 (0) 711 685 64241
E-mail: niewa@iac.uni-stuttgart.de

[a] Institut für Anorganische Chemie, Universität Stuttgart, Pfaffenwaldring 55, 70569 Stuttgart, Germany

[b] Technische Universität München, Department Chemie, Garching, Germany

[c] University of Kentucky, Department of Physics & Astronomy, Lexington, KY 40506-0055 USA

We have recently developed a technique for single-crystal growth of Ba-containing R -type ruthenium ferrites from a BaCl_2 flux [4]. Subsequently, we have adapted this method to grow single crystals of the Sr analogues having mm-sizes sufficient for structure determination and detailed studies of magnetic and electric properties. We find that these properties depend upon compositions that cover broad homogeneity ranges (i.e., Ru substitution by Fe and Co, and substitution by nonmagnetic elements such as Al) that we have established for the R -type structure.

Introduction

A prerequisite for applications of spin-polarized semiconductor devices is the development of suitable room-temperature, soft ferromagnetic semiconductors compatible with silicon-based components. Dilute magnetic semiconductors have been under intense study for applications in spintronics [1, 2]; however, the weak solubility of the randomly placed magnetic ions makes these materials unsuitable for devices. It is therefore crucial to identify and develop room-temperature ferromagnetic semiconductors based upon a periodic arrangement of magnetic moments (so-called “concentrated magnetic semiconductors”) [3].

Recently, we have discovered that R -type ferrites with general compositions $\text{BaFe}_{2\pm x}\text{Ru}_{4\mp x}\text{O}_{11}$ and $\text{SrFe}_{2\pm x}\text{Ru}_{4\mp x}\text{O}_{11}$ exhibit long-range ferromagnetic order well above room temperature, accompanied by narrow-gap semiconducting properties that include a large anomalous Hall conductance, low resistivity, and high carrier concentrations [4 – 6]. These properties are attractive for spintronic applications, and can be tuned by changing the composition (e.g., the Ru/Fe ratio). We found the compositions $\text{BaM}_{2\pm x}\text{Ru}_{4\mp x}\text{O}_{11}$ ($M = \text{Co}, \text{Fe}$) exhibit extended homogeneity ranges, and have analyzed the degree of order for Ru and M at various crystallographic sites. Herein we report crystallographic data on the Sr-phases, which have been unavailable in the literature, together with magnetic and transport measurement data.

Results and Discussion

Crystal structure and composition

$\text{BaM}_2\text{Ru}_4\text{O}_{11}$ compounds of the *R*-type hexagonal structure with $M = \text{Mn, Fe, Co}$ are known; the first report on $\text{BaFe}_2\text{Ru}_4\text{O}_{11}$ indicated the presence of mixed Fe–Ru occupation of all crystallographic positions occupied by transition metal atoms [7]. However, it was noted that Fe apparently prefers a trigonal bipyramidal coordination and Ru an octahedral environment. A recent detailed study [8] reported the structural, electrical and magnetic properties of microcrystalline samples of $\text{BaMn}_2\text{Ru}_4\text{O}_{11}$ and $\text{BaFe}_2\text{Ru}_4\text{O}_{11}$; samples were produced from “appropriate ratios” of starting materials and were found to be single-phase with the given ideal compositions. This work also focused on the Mn–Ru distribution in the crystal structure, and the magnetic structure of $\text{BaMn}_2\text{Ru}_4\text{O}_{11}$ was determined from neutron powder diffraction.

We have used our flux technique [4] to grow single crystals of novel $\text{SrM}_{2\pm x}\text{Ru}_{4\mp x}\text{O}_{11}$ phases that are isotypic with the *R*-type ferrites $\text{BaM}_{2\pm x}\text{Ru}_{4\mp x}\text{O}_{11}$ with $M = \text{Co, Fe}$. Tables 1 – 3 give selected data from our crystal structure refinements that yield compositions with $x = 0.54(5)$ ($\text{SrFe}_{2.54(5)}\text{Ru}_{3.46}\text{O}_{11}$), $x = 1.04(7)$ ($\text{SrFe}_{3.04(7)}\text{Ru}_{2.96}\text{O}_{11}$), $x = 1.47(6)$ ($\text{SrFe}_{3.47(6)}\text{Ru}_{2.53}\text{O}_{11}$) and $x = -0.11(8)$ ($\text{SrCo}_{1.89(8)}\text{Ru}_{4.11}\text{O}_{11}$).

We can view the hexagonal crystal structure as derived from *6H*-perovskites since Sr and O form a distorted hexagonal-close-packed motif with Sr located in anti-cuboctahedral coordination by O (see Fig. 1). However, occupation of additional octahedra by Ru and *M* (designated by *M*(1) and *M*(2) in the following), and concomitant replacement of Sr by O, leads to the so-called *R*-type structure with the general composition $\text{SrM}_{2\pm x}\text{Ru}_{4\mp x}\text{O}_{11}$. Additionally, trigonal bipyramids (*i.e.*, voids of two face-sharing tetrahedra denoted as *M*(3)) are exclusively occupied by Fe or Co, whereas the octahedra are jointly occupied by Ru and Fe or Co. The crystal structure is built up from (001) layers of edge-sharing octahedra surrounding *M*(2). The metal species form a Kagome net; *i.e.*, the layers contain unoccupied octahedral voids. These parallel (001) layers are connected along [001] via pairs of face-sharing octahedra centered by *M*(1) and the axial positions of the trigonal bipyramids centered around *M*(3).

The transition metal species on site *M*(3) exhibit an extreme elongation of their displacement ellipsoid in refinements in space group *P6₃/mmc*, which may indicate a dynamic or, more likely, a static displacement with statistical occupation of either one of two face-sharing tetrahedra. Refinements with a split position (as was suggested for isotypic $\text{BaTi}_2\text{Fe}_4\text{O}_{11}$ and $\text{BaSn}_2\text{Fe}_4\text{O}_{11}$ [9]) or, alternatively, in the corresponding non-centrosymmetric space group *P6₃mc*, did not lead to a significant improvement of the refinement. This applies also for a twin-refinement in *P6₃mc* with the (001) mirror plane implemented as a twin law. The non-centrosymmetric structure was observed for the isostructural vanadate $\text{PbV}_6\text{O}_{11}$ at ambient temperature, probably due to the steric influence of the lone pair of Pb^{2+} [10]. $\text{PbV}_6\text{O}_{11}$, as well as the corresponding vanadates $\text{NaV}_6\text{O}_{11}$ and $\text{SrV}_6\text{O}_{11}$, suffer a displacive phase transition from a centered to non-centered

structure with decreasing temperatures below 560 K (Pb), 245 K (Na) and 320 K (Sr), respectively [11].

As previously found for the Ba-isotypes [4], different levels of occupation (as compared to literature reports) of the two sites *M*(1) and *M*(2) with Ru and Fe or Co lead to deviations from the ideal composition $\text{SrM}_2\text{Ru}_4\text{O}_{11}$ – *i.e.*, a homogeneity range $\text{SrM}_{2\pm x}\text{Ru}_{4\mp x}\text{O}_{11}$ ($M = \text{Fe, Co}$) exists. Semiquantitative elemental analyses using the μ -probe technique yielded an atomic density ratio $n(\text{Ru})/n(\text{Fe}) = 1.52$ that corresponds to the composition $\text{SrFe}_{2.4}\text{Ru}_{3.6}\text{O}_{11}$, to be compared to the X-ray refinement result, $\text{SrFe}_{2.54(5)}\text{Ru}_{3.46}\text{O}_{11}$. The corresponding μ -probe results for other crystals are $n(\text{Ru})/n(\text{Fe}) = 1.11$ (*i.e.*, $\text{SrFe}_{2.8}\text{Ru}_{3.2}\text{O}_{11}$) for refined composition $\text{SrFe}_{3.04(7)}\text{Ru}_{2.96}\text{O}_{11}$, and $n(\text{Ru})/n(\text{Fe}) = 1.06$ (*i.e.*, $\text{SrFe}_{2.9}\text{Ru}_{3.1}\text{O}_{11}$) for refined composition $\text{SrFe}_{3.47(6)}\text{Ru}_{2.53}\text{O}_{11}$. The analysis for the Co-bearing crystal yielded a ratio of $n(\text{Ru})/n(\text{Co}) = 2.63$ (*i.e.*, $\text{SrCo}_{1.7}\text{Ru}_{4.3}\text{O}_{11}$) for refined composition $\text{SrCo}_{1.89(8)}\text{Ru}_{4.11}\text{O}_{11}$. Considering the limitations of the μ -probe technique, the resulting compositions are in reasonable agreement with the refinements of the X-ray diffraction data.

It should be noted that microprobe analysis also shows that several crystals (with compositions close to $\text{SrFe}_{2.54}\text{Ru}_{3.46}\text{O}_{11}$) contain Al at a concentration near 7 at% substitution for transition metal atoms. These crystals grew in contact with the side of an alumina crucible; therefore, we believe that the aluminum originates from the crucible. A site occupation with Ru and Fe is indistinguishable in the X-ray diffraction data refinements from a mixed occupation with the three elements, Ru, Fe and Al. Therefore, we cannot quantify the Al concentration in the *M*(1) or *M*(2) sites. On the other hand, the refinements indicate no Al in the *M*(3) sites. The crystal structure data and discussion are exclusively derived from crystals with no significant Al impurity. The reader should note that microprobe analysis in combination with the structure refinements leads to the composition $\text{SrFe}_{2.51}\text{Ru}_{3.42}\text{Al}_{0.07}\text{O}_{11}$ for the crystal studied in the *Magnetic and Transport Properties* section, below.

Ru shows a clear preference for the occupation of face-sharing octahedra, as opposed to edge- and corner-sharing octahedra, in ordered quaternary hexagonal perovskites [12]. Nevertheless, the *M*(1) position in the face-sharing octahedra exhibits a higher Fe occupation than the *M*(2) site for all studied compositions. A similar trend was observed for the isotypic Ba-compound $\text{BaFe}_{3.39(5)}\text{Ru}_{2.61}\text{O}_{11}$ [4]; however, for $\text{BaCo}_{1.85(6)}\text{Ru}_{4.15}\text{O}_{11}$ the opposite trend was observed, corresponding to the present results in the tables for $\text{SrCo}_{1.89(8)}\text{Ru}_{4.11}\text{O}_{11}$. The mixed occupation of both *M*(1) and *M*(2) sites for the Fe-bearing phases is approximately linear in composition and similar in slope, within the limited accuracy of data, from three samples with intermediate compositions (see Tables 2 and 3).

Interestingly, the unit cell parameter *a* for the title compounds is nearly independent of the composition ratio Ru/Fe (varying less than 0.7 % for the presented phases) and nearly matches that of the corresponding Ba compounds, with a difference of about –1.5 % [4]. This situation presents interesting possibilities for fabrication of epitaxial thin-film heterostructures. On the other hand, the lattice parameter *c* is sensitive to both substitution of Ba by Sr, and the Fe/Ru ratio within the octahedra. Taking into account the nearly identical distances and angles in the coordination of the

$M(2)$ sites within the (001) layers of octahedra, we can attribute the composition dependence of c to the Fe/Ru occupation of the face-sharing octahedra centered by the $M(1)$ site. Concurrently, the $M(2)O_6$ octahedra are compressed along [001], as indicated by internal angles.

The $M(1)$ atoms within the face-sharing octahedra show an increasing tendency to avoid each other with decreasing Ru content. The separation of these two Ru atoms was earlier shown to be indicative of the Ru oxidation state. The observed separation $d(M(1)-M(1)) \leq 2.7 \text{ \AA}$ is in the expected range for $Ru^{4.5}$ for the Fe compounds (Table 4) [13]. However, intermediate as well as mixed valences have been frequently observed for oxoruthenates [14], so we have to consider the possibility of different Ru oxidation states for sites $M(1)$ (face-sharing octahedra) and $M(2)$ (no face-sharing) in the R -type structure. In particular, $d(M(1)-M(1)) \approx 2.6 \text{ \AA}$ lies in the expected range for $Ru^{4.5}$ for $SrCo_{1.89(8)}Ru_{4.11}O_{11}$.

Magnetic and transport properties

Here, we report new data that confirm our previous finding that higher iron content corresponds to higher T_C 's [5, 6], and verify a linear dependence of the Curie temperature T_C of strontium ferrites on iron concentration [6] (Fig. 2). The wide homogeneity ranges accessible via $4d/3d$ -metal substitutions allow one to tune the strength of ferromagnetic interactions, anisotropy and T_C within the R -type structure [4]. As indicated above, several crystals obtained from growths conducted in Al_2O_3 crucibles also contain aluminum at concentrations near 7 at% substitution for transition metal atoms.

The temperature dependence of the magnetic susceptibility $\chi(T)$ of a $SrFe_{2.51}Ru_{3.42}Al_{0.07}O_{11}$ single crystal (Fig. 3) reveals a ferromagnetic (or possibly ferrimagnetic) transition anomaly at the Curie temperature $T_C = 305 \text{ K}$, close to the magnetic transition temperature of single-crystal $SrFe_{2.6}Ru_{3.4}O_{11}$ ($T_C = 300 \text{ K}$) [6]. We note that such Al doping levels do not affect the strong magnetization anisotropy $m_{\perp}/m_{\parallel} \approx 300$ characteristic of pure $SrFe_{2.6}Ru_{3.4}O_{11}$ at $T = 5 \text{ K}$. $M(H)$ curves for single-crystal $SrFe_{2.51}Ru_{3.42}Al_{0.07}O_{11}$ exhibit a typical ferromagnetic hysteresis without saturation in fields up to 5.5 T for both field directions (inset in Fig. 4). The small coercive fields $H_{c\parallel} \approx H_{c\perp} = 12 \text{ Oe}$ observed for single-crystal $SrFe_{2.51}Ru_{3.42}Al_{0.07}O_{11}$ are also very close to those observed for $SrFe_{2.6}Ru_{3.4}O_{11}$ [6].

We were not able to estimate the semiconducting gap of $SrFe_{3.04(7)}Ru_{2.96}O_{11}$ or $SrFe_{3.47(6)}Ru_{2.53}O_{11}$ since the sizes of the single-crystal samples were too small for transport measurements. Nevertheless, in-plane resistivity $\rho(T)$ of single-crystal $SrFe_{2.51}Ru_{3.42}Al_{0.07}O_{11}$ was obtained, and is shown in Fig. 4. The order-of-magnitude increase of the in-plane resistivity as the temperature falls from 300 to 5 K, and the slope $d\rho/dT < 0$, indicate semiconductivity. The corresponding resistivity of single-crystal $SrFe_{2.6}Ru_{3.4}O_{11}$ doubles over the same temperature interval. At temperatures above 180 K, $\rho(T)$ obeys an activated form $\rho_{\parallel} = \rho_0 e^{\Delta/kT}$ for current parallel to the **ab**-plane with narrow gaps, $\Delta \approx 30 \text{ meV}$ and 10 meV for $SrFe_{2.51}Ru_{3.42}Al_{0.07}O_{11}$ and $SrFe_{2.6}Ru_{3.4}O_{11}$, respectively. Therefore, the substitution of 7 at% transition metal atoms by Al increases the

semiconducting gap three-fold. The gap increase might indicate the localization of holes arising from substitution of magnetic Ru^{3+} , Ru^{5+}/Fe^{3+} by nonmagnetic Al^{3+} . Hall coefficient measurements reveal the predominant charge carriers in single-crystal $SrFe_{2.51}Ru_{3.42}Al_{0.07}O_{11}$ are holes (inset in Fig. 4). The addition of Al impurities approximately quadruples the anomalous contribution to the Hall effect of $SrFe_{2.51}Ru_{3.42}Al_{0.07}O_{11}$ at $T = 300 \text{ K}$, compared to single-crystal $SrFe_{2.6}Ru_{3.4}O_{11}$.

Figure 1. Crystal structure of $\text{SrM}_{2+x}\text{Ru}_{4-x}\text{O}_{11}$: Layers of $M(2)\text{O}_6$ octahedra (lighter octahedra) are connected in [001] direction *via* pairs of octahedra $M(1)_2\text{O}_9$ (darker octahedra) and trigonal prisms $(\text{Fe,Co})\text{O}_5$ (dark polyhedra centered by $M(3)$), respectively. Sr (large pale spheres) is located within the layers of pairs of octahedra and trigonal prisms.

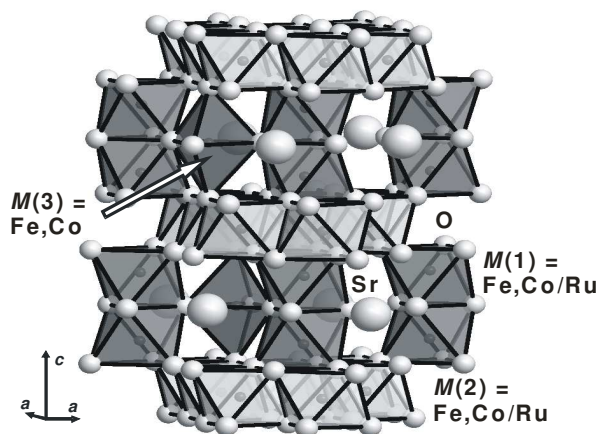


Figure 2. Fe concentration dependence of T_C for $\text{SrFe}_{2+x}\text{Ru}_{4-x}\text{O}_{11}$ data for single crystals with $x = 0.6$ or 0.8 , and a polycrystalline sample with $x = 1.04$ are from this work, the other data are taken from Ref. 6. The solid line is a linear fit to the data.

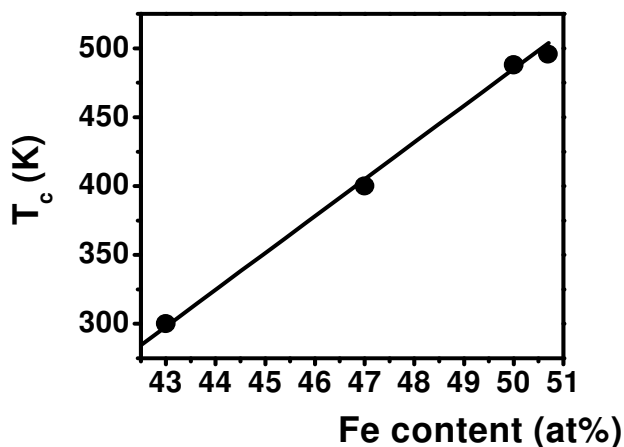


Figure 3. Temperature dependence of the FC DC magnetic susceptibility $\chi(T)$ of a single crystal with composition $\text{SrFe}_{2.51}\text{Ru}_{3.42}\text{Al}_{0.07}\text{O}_{11}$ for applied magnetic field $\mathbf{H} \parallel \mathbf{ab}$ (filled symbols) and $\mathbf{H} \perp \mathbf{ab}$ (empty symbols) for $\mu_0 H = 0.01$ T. The inset shows the magnetic moment m vs. H at 300 K.

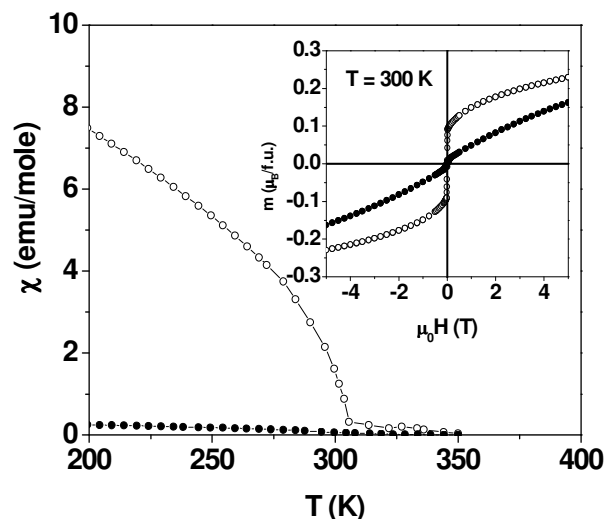


Figure 4. Temperature dependence of the resistivity $\rho(T)$ for $\text{SrFe}_{2.51}\text{Ru}_{3.42}\text{Al}_{0.07}\text{O}_{11}$ and $\text{SrFe}_{2.6}\text{Ru}_{3.4}\text{O}_{11}$ single crystals for electrical current $\mathbf{I} \parallel \mathbf{ab}$. The inset shows the magnetic field dependencies of the Hall resistivities $\rho_H(H)$ of these crystals at 300 K. The sharp change in slope at 0.1 T (anomalous Hall effect) is good evidence for a substantial electron spin-polarization.

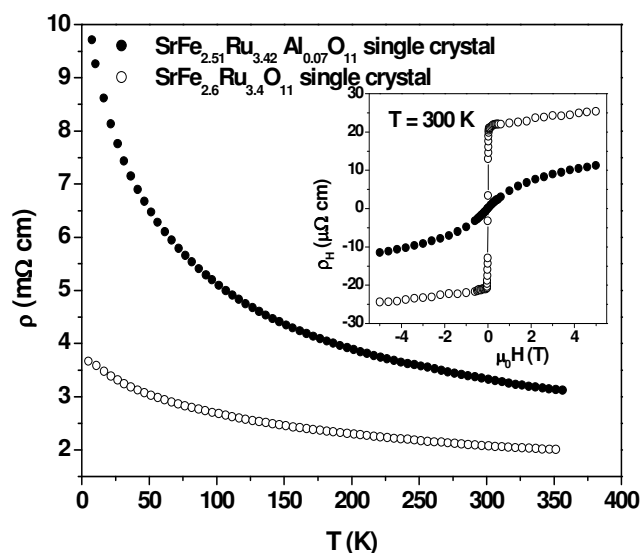


Table 1. Crystal structure data for single-crystal SrFe_{2.54(5)}Ru_{3.46}O₁₁, SrFe_{3.04(7)}Ru_{2.96}O₁₁, SrFe_{3.47(6)}Ru_{2.53}O₁₁ and SrCo_{1.89(8)}Ru_{4.11}O₁₁.

Formula	SrFe _{2.54(5)} Ru _{3.46} O ₁₁	SrFe _{3.04(7)} Ru _{2.96} O ₁₁	SrFe _{3.47(6)} Ru _{2.53} O ₁₁	SrCo _{1.89(8)} Ru _{4.11} O ₁₁
Cryst. size, mm ³	0.04 × 0.05 × 0.001	0.06 × 0.03 × 0.002	0.05 × 0.03 × 0.001	0.03 × 0.03 × 0.001
Crystal system	Hexagonal			
Space group	<i>P6₃/mmc</i>			
<i>a</i> , Å	5.8517(2)	5.8428(1)	5.8458(2)	5.8366(2)
<i>c</i> , Å	13.3171(4)	13.3546(2)	13.3981(3)	13.2730(11)
<i>V</i> , Å ³	394.91	394.82	396.52	391.58
<i>Z</i>	2			
<i>D</i> _{calcd} , g cm ⁻³	6.33	6.16	5.97	6.29
μ (MoK α), mm ⁻¹	17.73	17.70	17.59	18.44
<i>F</i> (000), e	688.6	670.6	655.1	715.74
<i>hkl</i> range	±10, ±10, -22 - 24	-7 - 5, ±7, ±17	±7, ±7, -17 - 15	±7, ±7, -15 - 17
2 θ _{max} , deg	82.96	55.65	55.60	55.31
Refl. measured	16868	10693	4089	5835
Refl. unique	554	215	215	211
<i>R</i> _{int}	0.042	0.033	0.034	0.029
Param. refined	28			
<i>R</i> (<i>F</i>)/ <i>wR</i> (<i>F</i> ²) (all reflections)	0.028/0.073	0.023/0.070	0.020/0.050	0.019/0.059
GoF (<i>F</i> ²)	1.127	1.195	1.294	1.056
$\Delta\rho$ _{fin} , e Å ⁻³	1.67	0.98	0.67	0.63

Table 2. Positional parameters for SrFe_{2.54(5)}Ru_{3.46}O₁₁ (first row of parameters), SrFe_{3.04(7)}Ru_{2.96}O₁₁ (second row of parameters in bold), SrFe_{3.47(6)}Ru_{2.53}O₁₁ (third row of parameters in italic) and SrCo_{1.89(8)}Ru_{4.11}O₁₁ (last row of parameters). *U*-values given in Å².

Atom	Site	<i>x</i>	<i>y</i>	<i>z</i>	<i>U</i> _{eq}
Sr(1)	2 <i>c</i>	1/3	2/3	1/4	0.0184(3)
					0.0183(5)
					<i>0.0149(4)</i>
					0.0230(6)
<i>M</i> (1)*	4 <i>e</i>	0	0	0.15061(4)	0.0083(2)
				0.14968(7)	0.0093(4)
				<i>0.14919(7)</i>	<i>0.0081(4)</i>
				0.15265(3)	0.0107(3)
<i>M</i> (2)*	6 <i>g</i>	1/2	0	0	0.0164(2)
					0.0151(4)
					<i>0.0134(3)</i>
					0.0195(3)
Fe(3)	2 <i>d</i>	2/3	1/3	1/4	0.0205(4)
					0.0243(6)
					<i>0.0233(6)</i>
Co(3)					0.0171(7)
O(1)	12 <i>k</i>	0.1720(3)	2 <i>x</i>	0.0828(2)	0.0149(5)
		0.1722(4)		0.0823(3)	0.0138(9)
		<i>0.1723(4)</i>		<i>0.0824(3)</i>	<i>0.0134(8)</i>
		0.1721(4)		0.0823(4)	0.018(1)
O(2)	6 <i>h</i>	0.3065(8)	1/2 <i>x</i>	1/4	0.0165(8)
		0.305(1)			0.016(1)
		<i>0.305(1)</i>			<i>0.014(1)</i>
		0.301(1)			0.024(2)
O(3)	4 <i>f</i>	2/3	1/3	0.4151(4)	0.019(1)
				0.4153(5)	0.020(2)
				<i>0.4156(5)</i>	<i>0.020(2)</i>
				0.4194(6)	0.026(2)

* For SrFe_{2.54(5)}Ru_{3.46}O₁₁: *M*(1) = 0.43(1) Fe, 0.57 Ru; *M*(2) = 0.23(1) Fe, 0.77 Ru,
 for SrFe_{3.04(7)}Ru_{2.96}O₁₁: *M*(1) = 0.53(1) Fe, 0.47 Ru; *M*(2) = 0.33(1) Fe, 0.67 Ru,
 for SrFe_{3.47(6)}Ru_{2.53}O₁₁: *M*(1) = 0.62(1) Fe, 0.38 Ru; *M*(2) = 0.41(1) Fe, 0.59 Ru,
 for SrCo_{1.89(8)}Ru_{4.11}O₁₁: *M*(1) = 0.12(2) Co, 0.88 Ru; *M*(2) = 0.22(2) Fe, 0.78 Ru.

Table 3. Displacement parameters for $\text{SrFe}_{2.54(5)}\text{Ru}_{3.46}\text{O}_{11}$ (first row of parameters), $\text{SrFe}_{3.04(7)}\text{Ru}_{2.96}\text{O}_{11}$ (second row of parameters in bold), $\text{SrFe}_{3.47(6)}\text{Ru}_{2.53}\text{O}_{11}$ (third row of parameters in italic) and $\text{SrCo}_{1.89(8)}\text{Ru}_{4.11}\text{O}_{11}$ (last row of parameters). U -values given in \AA^2 .

Atom	U_{11}	U_{22}	U_{33}	U_{23}	U_{13}	U_{12}
Sr(1)	0.0198(4)	U_{11}	0.0157(4)	0	0	$1/2 U_{11}$
	0.0194(6)		0.0160(7)			
	<i>0.0152(6)</i>		<i>0.0143(7)</i>			
$M(1)^*$	0.0233(8)		0.023(1)			
	0.0074(2)	U_{11}	0.0101(2)	0	0	$1/2 U_{11}$
	0.0084(5)		0.0110(5)			
$M(2)^*$	<i>0.0070(5)</i>		<i>0.0104(5)</i>			
	0.0110(4)		0.0099(4)			
	0.0146(2)	0.0361(3)	0.0058(2)	-0.0012(2)	$1/2 U_{23}$	$1/2 U_{22}$
Fe(3)	0.0141(4)	0.0306(5)	0.0062(4)	-0.0004(2)		
	<i>0.0120(4)</i>	<i>0.0265(5)</i>	<i>0.0064(4)</i>	<i>0.0002(3)</i>		
	0.0172(4)	0.0397(5)	0.0090(5)	-0.0029(4)		
Co(3)	0.0084(4)	U_{11}	0.0447(9)	0	0	$1/2 U_{11}$
	0.0085(8)		0.056(2)			
	<i>0.0058(7)</i>		<i>0.058(2)</i>			
O(1)	0.0101(8)		0.031(1)			
	0.0142(8)	0.014(1)	0.016(1)	0.0054(9)	$1/2 U_{23}$	$1/2 U_{22}$
	0.013(2)	0.014(2)	0.014(2)	0.004(1)		
O(2)	<i>0.012(1)</i>	<i>0.013(2)</i>	<i>0.016(2)</i>	<i>0.003(2)</i>		
	0.016(2)	0.020(2)	0.020(2)	0.003(2)		
	0.012(2)	0.027(2)	0.005(1)	0	0	$1/2 U_{11}$
O(3)	0.015(3)	0.023(2)	0.007(2)			
	<i>0.012(3)</i>	<i>0.018(2)</i>	<i>0.010(2)</i>			
	0.019(3)	0.037(3)	0.010(3)			
O(3)	0.024(2)	U_{11}	0.011(2)	0	0	$1/2 U_{11}$
	0.024(3)		0.011(3)			
	<i>0.022(3)</i>		<i>0.015(3)</i>			
	0.032(3)		0.014(3)			

* For $\text{SrFe}_{2.54(5)}\text{Ru}_{3.46}\text{O}_{11}$: $M(1) = 0.43(1)$ Fe, 0.57 Ru; $M(2) = 0.23(1)$ Fe, 0.77 Ru,
for $\text{SrFe}_{3.04(7)}\text{Ru}_{2.96}\text{O}_{11}$: $M(1) = 0.53(1)$ Fe, 0.47 Ru; $M(2) = 0.33(1)$ Fe, 0.67 Ru,
for $\text{SrFe}_{3.47(6)}\text{Ru}_{2.53}\text{O}_{11}$: $M(1) = 0.62(1)$ Fe, 0.38 Ru; $M(2) = 0.41(1)$ Fe, 0.59 Ru,
for $\text{SrCo}_{1.89(8)}\text{Ru}_{4.11}\text{O}_{11}$: $M(1) = 0.12(2)$ Co, 0.88 Ru; $M(2) = 0.22(2)$ Fe, 0.78 Ru.

Table 4. Selected distances (\AA) for $\text{SrFe}_{2.54(5)}\text{Ru}_{3.46}\text{O}_{11}$ (first values), $\text{SrFe}_{3.04(7)}\text{Ru}_{2.96}\text{O}_{11}$ (second values in bold), $\text{SrFe}_{3.47(6)}\text{Ru}_{2.53}\text{O}_{11}$ (third values in italic) and $\text{SrCo}_{1.89(8)}\text{Ru}_{4.11}\text{O}_{11}$ (last values), with estimated standard deviations in parentheses.

Sr(1)	-O(1)	2.762(3)	2.770(4)	2.776(4)	2.759(5)	6 ×
	-O(2)	2.9290(2)	2.9249(3)	2.9264(3)	2.9228(4)	6 ×
$M(1)$	- $M(1)$	2.647(1)	2.679(2)	2.702(2)	2.584(1)	1 ×
	-O(1)	1.963(3)	1.961(4)	1.961(4)	1.975(4)	3 ×
$M(2)$	-O(2)	2.041(3)	2.045(4)	2.052(4)	1.997(5)	3 ×
	-O(1)	1.995(2)	1.991(2)	1.993(3)	1.985(3)	4 ×
$M(3)$	-O(3)	2.033(3)	2.031(3)	2.031(3)	1.996(4)	2 ×
	-O(2)	1.826(4)	1.828(5)	1.830(6)	1.847(6)	3 ×
	-O(3)	2.198(5)	2.208(6)	2.219(7)	2.249(8)	2 ×

Summary and Conclusions

We report a series of soft ferromagnetic semiconductors $\text{SrM}_{2+x}\text{Ru}_{4-x}\text{O}_{11}$ ($M = \text{Fe, Co, Al}$) with T_C at or above room-temperature and extend the homogeneity range of the R -type ferrite phases. The small composition dependence of the hexagonal unit cell parameter a , coupled with promising electronic properties, offers a potential to fabricate epitaxial multilayer heterostructures having a range of compositions

and desirable electrical and magnetic properties without significant residual strain. Our results indicate that Al doping is effective in modifying the transport properties of strontium ferrites. On the other hand, magnetic properties such as the Curie temperature, magnetization and anisotropy are less affected by doping with Al. Therefore, these materials promise to be compatible with aluminum oxide surfaces that are common in semiconducting devices. In particular, solid solutions formed from Sr-based, R -type

ferrites with transition metal elements may lead to practical materials suitable for spin-injection devices.

Experimental Section

Preparation

Single crystals were prepared by mixing different molar ratios of SrCO₃, RuO₂ and Fe₂O₃ (or Co₃O₄) with SrCl₂, which was used as an agent to initiate crystal growth. The powders were heated in alumina or zirconia crucibles to 1350 °C and kept at this temperature for several days, after which the furnace was slowly cooled to room temperature. Black hexagonal platelets with maximal sizes of 2 mm and a thickness of about 0.05 mm were obtained.

Structure determination

Crystals in the form of small, black, hexagonal platelets were selected for X-ray diffraction data collection. The measurements were performed on an Oxford Xcalibur Diffractometer equipped with a graphite monochromator using MoK_α radiation, and a sapphire CCD area detector held at ambient temperature [Scans: Fe: φ (360 images, $\Delta\varphi = 1.0^\circ$, 5 s), ω (416 images, $\Delta\omega = 1.0^\circ$, 5 s), Co: φ (180 images, $\Delta\varphi = 2.0^\circ$, 30 s), ω (208 images, $\Delta\omega = 2.0^\circ$, 30 s)]. After empirical absorption correction, the structures were successfully solved using direct methods, and refined in space group *P6₃/mmc* (No. 194, centrosymmetric, program SHELXS-97-2 [15], SHELXL-97-2 [16]). Additional information on data collection, structure determinations and refinements is presented in Table 1. Tables 2 and 3 give positional parameters, site occupation numbers and displacement parameters.

Chemical composition

Chemical μ -probe analyses (JEOL 5900LV operating at 20 kV and equipped with a LINK AN 10000 detector system for EDX analysis) yielded very stable compositions (both for different crystals and several different sampling locations on every investigated crystal) having the approximate atomic ratio $n(M)/n(\text{Sr}) = 6.0$ in every case. This result also applies to crystals measured on the diffractometer. No reliable quantification of the oxygen content is possible with this technique. Except for some samples that were found to contain Al (probably originating from the crucible material), no additional elements were detected.

Transport properties measurements

The magnetic properties of oriented single crystals were measured using a Quantum Design MPMS5 SQUID Magnetometer operating over a temperature range 2 K to 400 K, or using a MPMS5 high-temperature oven accessory that operates from 300 K to 700 K. The resistivity and Hall effect were measured via a conventional four-probe method using the MPMS5 External Device Control Option, a Keithley Model 220 Current Source and Keithley Model 182 Nanovoltmeter with DC currents (0.1 mA to 20 mA) applied parallel or perpendicular to the sample **ab**-plane.

Supporting Information Further details of the crystal structure investigations may be obtained from Fachinformationszentrum Karlsruhe, 76344 Eggenstein-Leopoldshafen, Germany (fax: +49-7247-808-666; e-mail: crysdata@fiz-karlsruhe.de, http://www.fiz-informationsdienste.de/en/DB/icsd/depot_anforderung.html) on

quoting the deposition numbers CSD-420770 (SrFe_{2.54(5)}Ru_{3.46}O₁₁), CSD-420771 (SrFe_{3.04(7)}Ru_{2.96}O₁₁), CSD-420772 (SrFe_{3.47(6)}Ru_{2.53}O₁₁) and CSD-420773 (SrCo_{1.89(8)}Ru_{4.11}O₁₁).

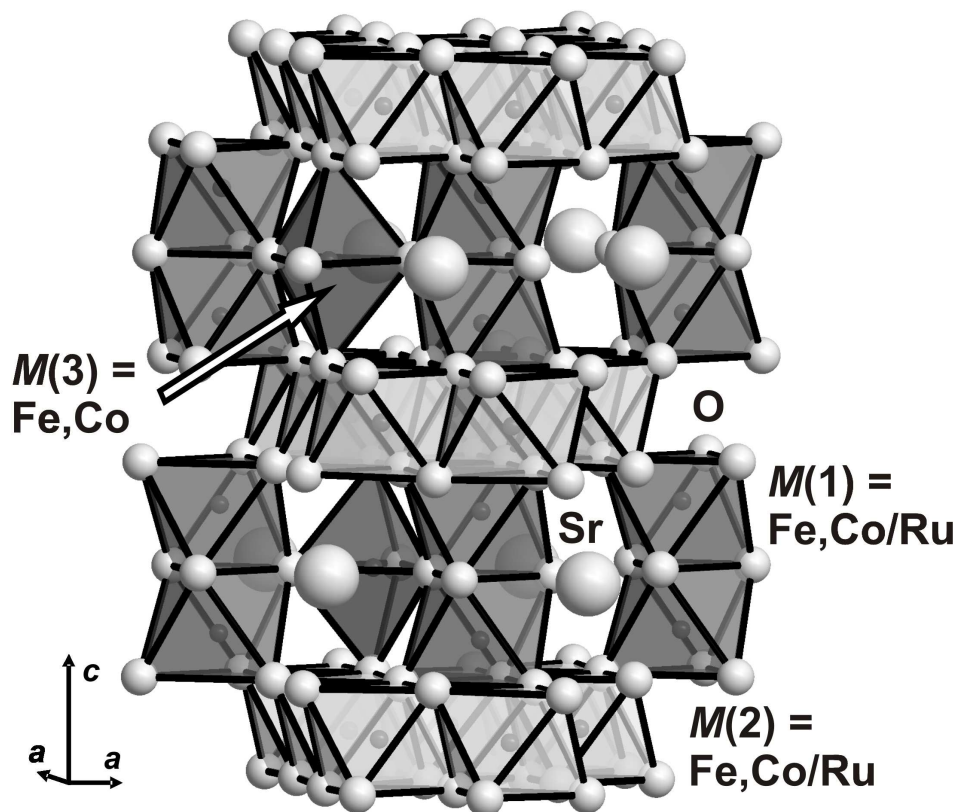
Acknowledgments

We thank Ingrid Werner (TU München) for performing the μ -probe measurements. Research at the University of Kentucky was supported by Kentucky Science and Engineering Foundation Grant #KSEF-1470-RDE-010 and U.S. DoE Grant #DOE-FG02-97ER45653.

- [1] I. Zutic, J. Fabian, S. Das Sarma, *Rev. Mod. Phys.* **2004**, *76*, 323-410.
- [2] D. D. Awschalom, M. E. Flatte, *Nature Physics* **2007**, *3*, 153-159.
- [3] T. Kasuya, A. Yanase, *Rev. Mod. Phys.* **1968**, *40*, 684-696.
- [4] B. Schüpp-Niewa, L. Shlyk, S. Kryukov, L. De Long, R. Niewa, *Z. Naturforsch. b* **2007**, *62*, 753-758.
- [5] L. Shlyk, L. E. De Long, S. Kryukov, B. Schüpp-Niewa, R. Niewa, *J. Appl. Phys.* **2008**, *103*, 07D112.
- [6] L. Shlyk, S. Kryukov, B. Schüpp-Niewa, R. Niewa, L. E. De Long, *Adv. Mater.* **2008**, *20*, 1315-1320.
- [7] D. Verdoes, H. W. Zandbergen, D. J. W. Ijdo, *Mater. Res. Bull.* **1987**, *22*, 1-10.
- [8] M. L. Foo, Q. Huang, J. W. Lynn, W.-L. Lee, T. Klimczuk, I. S. Hagemann, N. P. Ong, R. J. Cava, *J. Solid State Chem.* **2006**, *179*, 563-572.
- [9] M. C. Cadée, D. J. W. Ijdo, *J. Solid State Chem.* **1984**, *52*, 302-312.
- [10] O. Mentre, F. Abraham, *J. Solid State Chem.* **1996**, *125*, 91-101.
- [11] H. Kato, M. Kato, K. Yoshimura, K. Kosuge, *J. Phys.: Condens. Matter.* **2001**, *13*, 9311-9333.
- [12] B. Schüpp-Niewa, L. Shlyk, Yu. Prots, R. Niewa, G. Krabbes, *Z. Anorg. Allg. Chem.* **2006**, *632*, 572-576.
- [13] B. Schüpp-Niewa, L. Shlyk, Y. Prots, G. Krabbes, *J. Alloys Compd.* **2006**, *414*, 269-275.
- [14] Hk. Müller-Buschbaum, *Z. Anorg. Allg. Chem.* **2006**, *632*, 1625-1659.
- [15] G. M. Sheldrick, SHELXS-97-2, Program for the Solution of Crystal Structures, Universität Göttingen, Göttingen, Germany, 1997.
- [16] G. M. Sheldrick, SHELXL-97-2, Program for the Refinement of Crystal Structures, Universität Göttingen, Göttingen, Germany, 1997.

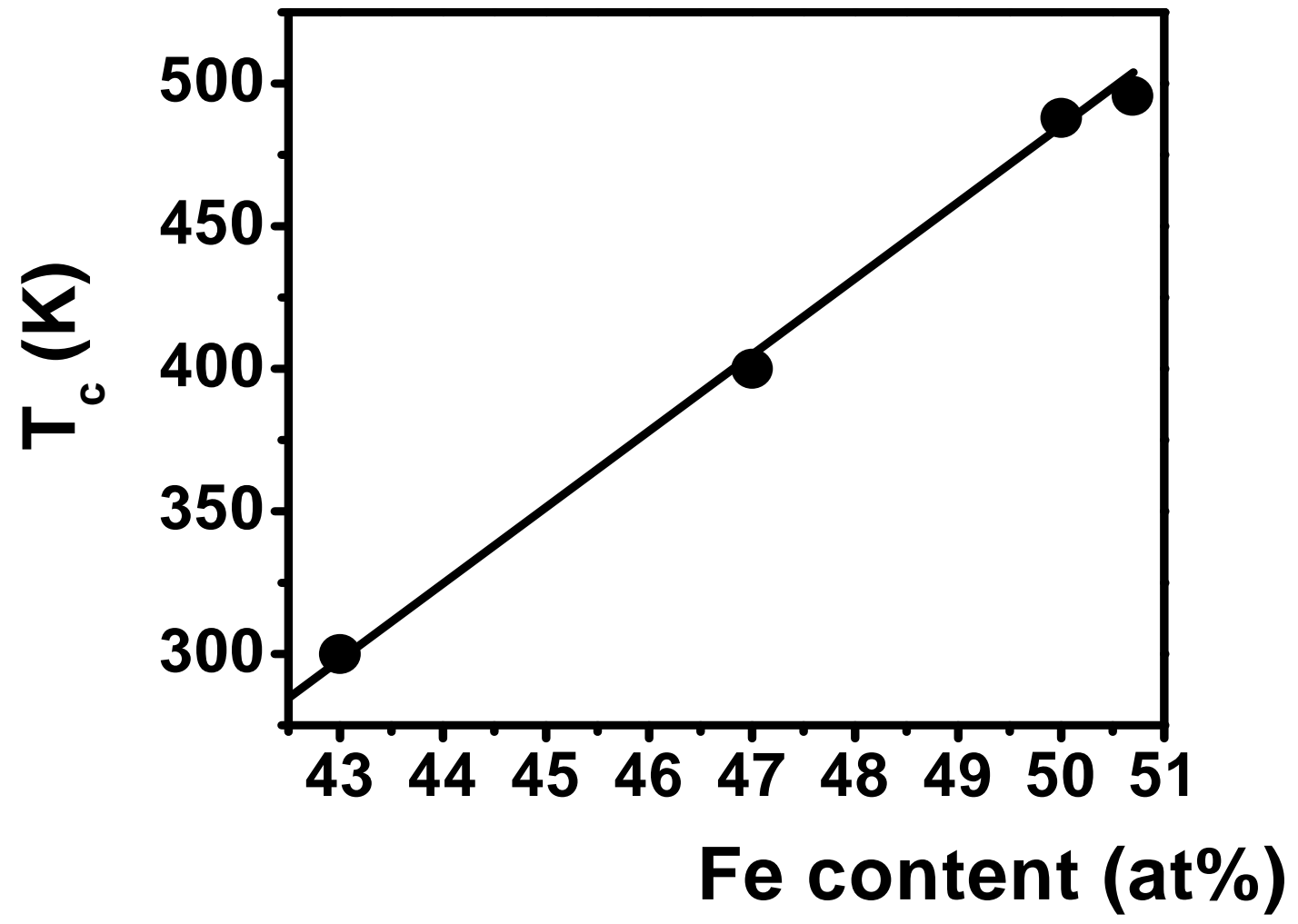
Received: ((will be filled in by the editorial staff))
Published online: ((will be filled in by the editorial staff))

1
2
3
4
5
6
7
8
9
10
11
12
13
14
15
16
17
18
19
20
21
22
23
24
25
26
27
28
29
30
31
32
33
34
35
36
37
38
39
40
41
42
43
44
45
46
47
48
49
50
51
52
53
54
55
56
57
58
59
60



Crystal structure of $\text{SrM}_{2\pm x}\text{Ru}_{4\pm x}\text{O}_{11}$: Layers of $M(2)\text{O}_6$ octahedra (lighter octahedra) are connected in $[001]$ direction via pairs of octahedra $M(1)_2\text{O}_9$ (darker octahedra) and trigonal prisms $(\text{Fe,Co})\text{O}_5$ (dark polyhedra centered by $M(3)$), respectively. Sr (large pale spheres) is located within the layers of pairs of octahedra and trigonal prisms.

197x178mm (300 x 300 DPI)



1
2
3
4
5
6
7
8
9
10
11
12
13
14
15
16
17
18
19
20
21
22
23
24
25
26
27
28
29
30
31
32
33
34
35
36
37
38
39
40
41
42
43
44
45
46
47

